Proceedings of ASME Turbo Expo 2011
GT2011
June 6-10, 2011, Vancouver, British Columbia, Canada

GT2011-45139

STATISTICAL AND THEORETICAL MODELS OF INGESTION THROUGH TURBINE RIM SEALS

Kunyuan Zhou[1] **Simon N Wood**[2] **J Michael Owen**[3]

[1] Dept. of Engineering Thermophysics
School of Jet Propulsion
Beihang University
Beijing, 100191 P.R.China

[2] Dept. of Mathematical Sciences
University of Bath
Bath, BA2 7AY
United Kingdom

[3] Dept. of Mechanical Engineering
University of Bath
Bath, BA2 7AY
United Kingdom

ABSTRACT

In recent papers, orifice models have been developed to calculate the amount of ingestion, or ingress, that occurs through gas-turbine rim seals. These theoretical models can be used for externally-induced (EI) ingress, where the pressure differences in the main gas path are dominant, and for rotationally-induced (RI) ingress, where the effects of rotation in the wheel-space are dominant. Explicit ‘effectiveness equations’, derived from the orifice models, are used to express the flow rate of sealing air in terms of the sealing effectiveness. These equations contain two unknown terms: Φ_{min}, a sealing flow parameter, and Γ_c, the ratio of the discharge coefficients for ingress and egress. The two unknowns can be determined from concentration measurements in experimental rigs.

In this paper, maximum likelihood estimation is used to fit the effectiveness equations to experimental data and to determine the optimum values of Φ_{min} and Γ_c. The statistical model is validated numerically using noisy data generated from the effectiveness equations, and the simulated tests show the dangers of drawing conclusions from sparse data points. Using the statistical model, good agreement between the theoretical curves and several sets of previously-published effectiveness data is achieved for both EI and RI ingress. The statistical and theoretical models have also been used to analyse previously-unpublished experimental data, the results of which are included in separate papers. It is the ultimate aim of this research to apply the effectiveness data obtained at rig conditions to engine-operating conditions.

NOMENCLATURE

A	area
b	radius of seal
$C_{d,e}, C_{d,i}$	discharge coefficients for egress, ingress
C_w	nondimensional flow rate ($=\dot{m}/\mu b$)
$C_{w,e}, C_{w,i}$	values of C_w for egress, ingress
$C_{w,o}$	nondimensional sealing flow rate
$C_{w,min}$	minimum value of $C_{w,o}$ to prevent ingress
e_j	j^{th} measured value of ε
G_c	seal-clearance ratio ($=s_c/b$)
l	log likelihood function
m	number of repeated tests
$\dot{m}$	mass flow rate
n	number of data points
N	normal distribution
p	absolute static pressure
r	radius
Re_ϕ	rotational Reynolds number ($=\rho\Omega b^2/\mu$)
s_c	seal clearance
U	bulk mean velocity of sealing flow ($=\dot{m}_o/2\pi\rho b s_c$)
V_r, V_ϕ	radial and tangential components of velocity
z	axial distance in seal clearance
δ	error
ΔC_p	nondimensional pressure difference
η_t	sealing flow parameter ($= 0.5Gc\, Re_\phi^{0.2}\Phi_o$)
γ	Γ_c^{-1}
Γ_c	ratio of discharge coefficients ($=C_{d,i}/C_{d,e}$)
$\hat{\Gamma}_c$	estimated value of Γ_c
$\bar{\Gamma}_c$	ensemble average of Γ_c
ε	sealing effectiveness ($=1-C_{w,i}/C_{w,e}$)
λ	parameter for calculation of confidence interval
μ	dynamic viscosity
ρ	density
$\boldsymbol{\theta}$	generic parameter vector
σ	standard deviation
ϕ_j	j^{th} value of Φ_o
Φ	sealing flow parameter ($=C_w/2\pi G_c Re_\phi$)
Φ_e	value of Φ when $C_w=C_{w,e}$ ($=C_{w,e}/2\pi G_c Re_\phi$)
Φ_i	value of Φ when $C_w=C_{w,i}$ ($=C_{w,i}/2\pi G_c Re_\phi$)
Φ_{min}	value of Φ_o when $C_{w,o}=C_{w,min}$ ($=C_{w,min}/2\pi G_c Re_\phi$)
$\hat{\Phi}_{min}$	estimated value of Φ_{min}
$\bar{\Phi}_{min}$	ensemble average of $\hat{\Phi}_{min}$

Φ_o value of Φ when $C_w=C_{w,o}$ $(=C_{w,o}/2\pi G_c Re_\phi)$
Ω angular velocity of rotating disc

Subscripts

e egress
EI externally-induced ingress
i ingress
j j^{th} data point
max maximum
min minimum
o sealing flow
RI rotationally-induced ingress
Γ relating to Γ_c
Φ relating to Φ_{min}
$1,2$ locations in wheel-space and annulus
$*$ value when $C_{w,o}=0$

1. INTRODUCTION

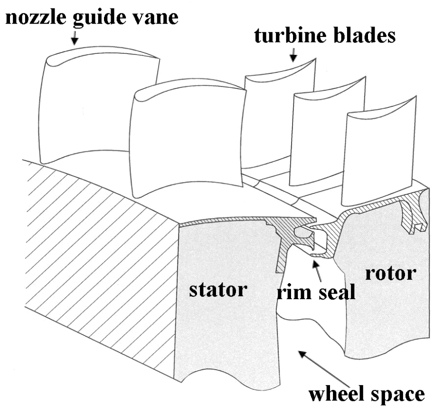

Fig. 1 Typical rim seal for high-pressure gas-turbine stage

Fig. 1 illustrates a typical high-pressure gas-turbine stage showing the rim seal and the wheel-space between the stator and the rotating turbine disc. The flow past the stationary vanes and rotating blades in the turbine annulus creates an unsteady 3D variation of pressure radially outward of the rim seal. Ingress and egress occur through those parts of the seal clearance where the external pressure is higher and lower, respectively, than that in the wheel-space. This non-axisymmetric type of ingestion is referred to here as *externally-induced* (EI) ingress.

Even when the external flow is axisymmetric, so that there is no circumferential variation of external pressure, ingress can still occur. The reason for this is that the rotating fluid in the wheel-space creates a radial gradient of pressure, so that the pressure inside the wheel-space can drop below that outside. The so-called 'disc-pumping effect' causes a radial outflow of fluid, or egress, near the rotating disc, and the low pressure in the wheel-space causes ingress of external fluid through the rim seal into the wheel-space. This axisymmetric type of ingestion is referred to here as *rotationally-induced* (RI) ingress, and Fig. 2 shows a simplified diagram of ingress and egress through an axial-clearance rim seal.

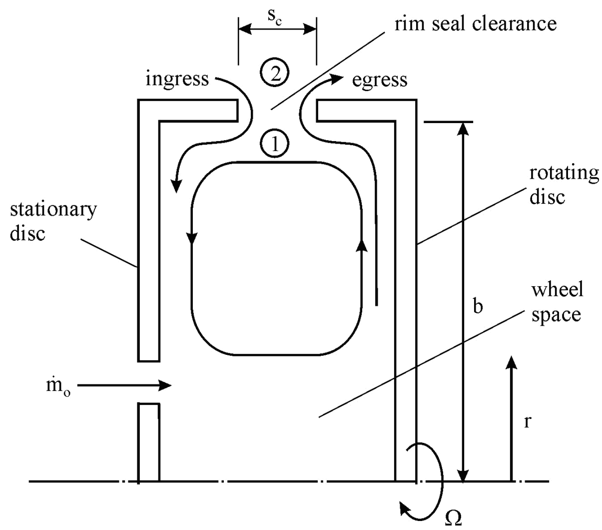

Fig. 2 Simplified diagram of ingress and egress

Although the sealing air can reduce ingress, too much air reduces the engine efficiency and too little can cause serious overheating, resulting in damage to the turbine rim and blade roots. The engine designer needs to know the value of $C_{w,min}$, the nondimensional sealing flow rate necessary to prevent ingress. If $C_{w,o}$, the nondimensional sealing flow rate, is less than $C_{w,min}$, the designer wants to know how much ingress occurs and how does the ingested fluid affect the temperatures in the wheel-space.

Owen and his co-workers [1-4] have developed orifice models for EI and RI ingress to calculate the effectiveness of gas-turbine rim seals. In principle, and within the limits of dimensional similitude, the models could be used to extrapolate measurements of sealing effectiveness made on an experimental rig at one set of operating conditions to an engine operating at another set of conditions.

Experimenters often use concentration measurements to determine the variation of ε, the sealing effectiveness, with $C_{w,o}$. It is the principal objective of this paper to show how statistical techniques can be used to fit the theoretical 'effectiveness equations', derived from the EI and RI orifice models, to the data obtained from experimental rigs. Using the parameters obtained from the fitted curves, the models should then be able to estimate the effectiveness at engine conditions.

As ingress has been reviewed in many recent papers, including references [1-4], only a brief review of the papers that are relevant to this study is included in Section 2. Section 3 explains the statistical fitting technique, Section 4 describes some numerical tests carried out on the technique, Section 5 shows how the technique can be applied to experimental data, and the principal conclusions are summarized in Section 6.

2. BRIEF REVIEW OF PREVIOUS WORK

Only a brief review of the ingress literature, including the papers that are used to validate the statistical and theoretical models described in this paper, is given here. More extensive reviews are given in [1-4].

2.1 RI and EI ingress

For RI ingress, Bayley and Owen [5] presented experimental results for a simple rotor-stator system with an axial-clearance rim seal in which there was a superposed radial flow of air that discharged through the seal into the atmosphere; there was no external annulus on the rig. Owing to the sub-atmospheric pressure created by the rotating flow in the system, external (atmospheric) air could be drawn into the wheel-space. Increasing the superposed flow rate increased the relative pressure inside the wheel-space and consequently reduced the amount of ingested air. At sufficiently high superposed flow rates, where $C_{w,o} \geq C_{w,min}$, ingress did not occur. Bayley and Owen used their measured pressures for G_c= 0.0033 and 0.0067, and for $Re_\phi \leq 4\times10^6$, to provide the correlation:

$$C_{w,min}=0.61 G_c\, Re_\phi \qquad (2.1)$$

Graber *et al.* [6] reported extensive concentration measurements in a rotating-disc rig, which was used to determine the effects of seal geometry, rotational Reynolds numbers and the level of swirl in the external annulus on ε, the sealing effectiveness. Their measurements, which showed that the external swirl had no systematic effect on the effectiveness, were used in [1] to validate the orifice model for RI ingress.

Phadke and Owen [7-9] conducted experiments for RI and EI ingress in a rotating-disc rig with a number of different rim-seal geometries. They showed that EI ingress was controlled by the peak-to-trough pressure difference in the annulus and that there was a transition from RI to EI ingress as the pressure difference was increased. This transition, in which the effects of rotation and external pressure difference are both significant, was referred to by Owen *et al.* [4], as *combined ingress*. They also showed that the orifice models could be used for this transitional form of ingestion.

For EI ingress, Johnson *et al.* [10] used an orifice model to obtain good estimates of the effectiveness measurements in the turbine rig of Bohn *et al.* [11]. They used the values obtained from 2D time-dependent CFD to determine the external circumferential pressure distribution used in their model, which allowed the effects of the vanes and blades to be taken into account. A modified version of their orifice model was also applied by Johnson *et al.* [12] to the ingress measurements made on a turbine rig in Arizona State University.

2.2 Orifice model for EI and RI ingress

The mathematical model for the orifice equations derived in [1] is based on an *orifice ring*, as shown in Fig. 3 for an axial-clearance seal, where ingress and egress simultaneously cross different parts of an imaginary ring. (The orifice ring can be thought of as a thin circular membrane with the same dimensions as the seal clearance.) Egress flows through a stream tube in the wheel-space where the static pressure is p_1 and, after crossing the ring through a small orifice with an area δA_e, emerges in the external annulus where the static pressure is p_2; conversely, ingress originates in the annulus and, after crossing the ring through an orifice with an area δA_i, emerges in the wheel-space.

It is assumed that there is continuity of mass and energy inside the separate stream tubes for egress and ingress but there is a discontinuity in the pressure across the sealing ring. In addition, angular momentum is conserved, so that free-vortex flow occurs and rV_ϕ is constant. The principal 'orifice assumptions' are that $(r_2-r_1)/r_1<<1$ and that $V_{r,1}^2<<V_{r,2}^2$ for egress and *vice versa* for ingress. Although the equations are derived for inviscid incompressible flow, discharge coefficients, analogous to those used for the standard orifice equations, are introduced to account for losses. In general, different discharge coefficients ($C_{d,i}$ and $C_{d,e}$) are needed for ingress and egress, and these have to be determined empirically.

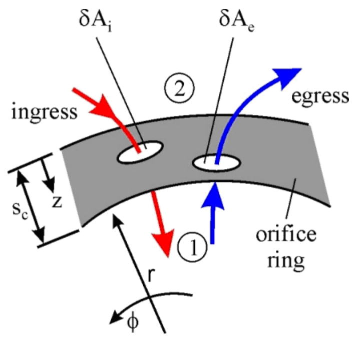

Fig. 3 Schematic of orifice model [1]

For rotationally-induced (RI) ingress, the flow is assumed to be axisymmetric: swirl of the flow in the wheel-space is included but external pressure asymmetries are ignored. For EI ingress, the circumferential variation of pressure in the annulus is included but swirl in the wheel-space is ignored. To obtain analytical solutions for EI ingress, the circumferential variation of pressure in the annulus was approximated in [2] by a linear saw-tooth model.

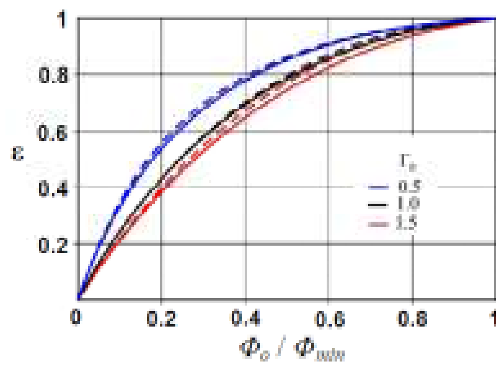

Fig. 4 Effect of Γ_c on variation of ε with Φ_o predicted by orifice models [2].
Solid line, EI ingress; dashed line, RI ingress.

Implicit relationships between the sealing effectiveness ε and the sealing flow parameter Φ_o were derived in [1, 2]. More convenient explicit relationships, referred to as the effectiveness equations, were derived for both EI and RI ingress and applied to experimental data by Sangan et al [13, 14]. The sealing flow parameter, which is useful for both EI and RI ingress, is usually defined as

$$\Phi_o = \frac{C_{w,o}}{2\pi G_c \, Re_\phi} \tag{2.2}$$

As Re_ϕ and $C_{w,o}$ include viscous terms, which cancel in eq (2.2), the above definition might give the misleading impression that viscosity has a role to play. An alternative definition is

$$\Phi_o = \frac{U}{\Omega b} \tag{2.3}$$

where U is the bulk mean radial velocity of sealing air through the seal clearance, so that

$$U = \frac{\dot{m}_o}{2\pi\rho b s_c} \tag{2.4}$$

Eq (2.3), apart from being simpler, clearly shows that Φ_o is an inertial parameter. Φ_{min} is the value of Φ_o when the system is sealed, so that $C_{w,o}=C_{w,min}$.

For RI ingress, the effectiveness equation for $\Phi_o \le \Phi_{min,RI}$ is

$$\frac{\Phi_o}{\Phi_{min,RI}} = \frac{\varepsilon}{[1+(1-\varepsilon)^{1/2}][1+\Gamma_c^{-2}(1-\varepsilon)]^{1/2}} \tag{2.5}$$

where Γ_c is the ratio of the discharge coefficients for ingress and egress, and $\varepsilon=1$ for $\Phi_o > \Phi_{min,RI}$. The designer is also interested in calculating the flow rate of ingested fluid that occurs when $\Phi_o < \Phi_{min,RI}$. As

$$\frac{\Phi_{i,RI}}{\Phi_o} = \varepsilon^{-1} - 1 \tag{2.6}$$

then it follows that

$$\frac{\Phi_{i,RI}}{\Phi_{min,RI}} = \frac{1-\varepsilon}{[1+(1-\varepsilon)^{1/2}][1+\Gamma_c^{-2}(1-\varepsilon)]^{1/2}} \tag{2.7}$$

and

$$\Phi_{i,RI}{}^* = \Phi_{min,RI}\,\frac{1}{2[1+\Gamma_c^{-2}]^{1/2}} \tag{2.8}$$

where $\Phi_{i,RI}$ is the nondimensional ingested flow rate and $\Phi_{i,RI}{}^*$ is the value of $\Phi_{i,RI}$ when $\Phi_o=0$. $\Phi_{i,RI}{}^*$ represents the maximum value of the nondimensional ingested flow rate.

For EI ingress, the effectiveness equation for $\Phi_o \le \Phi_{min,EI}$ is:

$$\frac{\Phi_o}{\Phi_{min,EI}} = \frac{\varepsilon}{[1+\Gamma_c^{-2/3}(1-\varepsilon)^{2/3}]^{3/2}} \tag{2.9}$$

and $\varepsilon=1$ for $\Phi_o > \Phi_{min,EI}$. As

$$\frac{\Phi_{i,EI}}{\Phi_o} = \varepsilon^{-1} - 1 \tag{2.10}$$

then the ingested flow rate can be calculated from

$$\frac{\Phi_{i,EI}}{\Phi_{min,EI}} = \frac{1-\varepsilon}{[1+\Gamma_c^{-2/3}(1-\varepsilon)^{2/3}]^{3/2}} \tag{2.11}$$

and

$$\Phi_{i,EI}{}^* = \Phi_{min,EI}\,\frac{1}{[1+\Gamma_c^{-2/3}]^{3/2}} \tag{2.12}$$

Fig. 4, which was adapted from [2], shows the effect of Γ_c on the variation of ε with Φ_o/Φ_{min} for EI and RI ingress. It can be seen that Γ_c affects the shape of the curves and, for a given value of Φ_o, the effectiveness decreases as Γ_c increases (that is, as $C_{d,i}$ increases). For the designer, Φ_{min} (which determines how much sealing air is required to prevent ingress) is more important than Γ_c. The statistical model described below allows the effectiveness equations to be fitted to experimental data in order to find the best estimates of Φ_{min} and Γ_c.

3. FITTING STATISTICAL MODEL TO DATA

3.1 Maximum likelihood estimation

For simplicity, the subscripts EI and RI are not used in this section.

Different values of the parameters Γ_c and Φ_{min} in the effectiveness equations (2.5) and (2.9) lead to different curves. The aim of statistical model estimation is to find the values, or a range of values, of Γ_c and Φ_{min} that lead to curves that best match empirical data on how ε varies with Φ_o. We will do this by maximum likelihood estimation. This is the standard method which, due to its favourable properties and wide applicability, is preferred by statisticians. Wood [15] gives an introduction to the method, and more details are given by Silvey [16] and by Davison [17].

Consider a set of measurements of ε as Φ_o is varied experimentally. Let e_j denote the measured value of ε, corresponding to the j^{th} value of Φ_o, which is denoted by ϕ_j. Furthermore let $\varepsilon(\Gamma_c, \Phi_{min}, \phi_j)$ denote the *model predicted* value of ε corresponding to ϕ_j, when the parameter values are Γ_c and Φ_{min}. For any given $\Gamma_c, \Phi_{min}, \phi_j$ values, ε can always be obtained from eqs (2.5) or (2.9) by numerical root finding (see e.g. [18]).

To obtain a statistical model we suppose that the measurements e_j can be modelled as noisy observations of ε. Specifically, we assume that e_j is normally distributed around a mean $\varepsilon(\Gamma_c, \Phi_{min}, \phi_j)$ with variance, σ^2. That is, $e_j \sim N(\varepsilon(\Gamma_c, \Phi_{\min}, \phi_j), \sigma^2)$.

We further assume that the e_j are statistically independent (i.e. knowing the value of e_1 provides no more information about e_2 than we already had from knowing ϕ_2). Under these assumptions we can write down the *joint* *probability density function f* for the whole vector $\boldsymbol{e}$ of e_j values, given the ϕ_j and the parameter values, namely

$$f(\boldsymbol{e})=(2\pi\,\sigma^2)^{-n/2}exp\left\{-\sum[e_j-\varepsilon(\Gamma_c,\Phi_{min},\ \phi_j)]^2/2\,\sigma^2\right\} \tag{3.1}$$

where n is the number of observations or data points.

The key idea of maximum likelihood estimation is that the values of the parameters (here Γ_c, Φ_{min} and σ) most likely to be correct are those that maximize the probability of the data according to eq (3.1). The method proceeds by putting the observed values of e_j and ϕ_j into the right-hand-side of eq (3.1), and treating the resulting expression as a function of the parameters Γ_c ,Φ_{min} and σ. This function is known as the *likelihood function* of the parameters.

For practical and theoretical convenience it is better to work with the log of the likelihood function, denoted by l. In this case,

$$l(\Gamma_c,\Phi_{min},\ \sigma)=-n/2log(2\pi)-nlog(\sigma)-\sum[e_j-\varepsilon(\Gamma_c,\Phi_{min},\ \phi_j)]^2/(2\,\sigma^2) \tag{3.2}$$

l measures the consistency of the experimental data and the model curves generated by particular parameter values; note the link with least squares here. The values of the parameters which maximize l are the *maximum likelihood estimates* of the parameters, denoted by $\hat{\Gamma}_c$, $\hat{\Phi}_{min}$ and $\hat{\sigma}$. These can be obtained numerically by variants of Newton's method or Downhill Simplex (see e.g. Nocedal and Wright [19]) .

Let $\boldsymbol{\theta}$ denote a generic parameter vector (here $(\Gamma_c, \Phi_{min}, \sigma)^T$), with log likelihood l. It can be shown (see e.g. [15, 16]) that in the limit $n \rightarrow \infty$,

$$\hat{\boldsymbol{\theta}} \sim N(\boldsymbol{\theta}, -(\partial^2 l/\partial\boldsymbol{\theta}\partial\boldsymbol{\theta}^T)^{-1}) \tag{3.3}$$

That is, with a large number of repeated tests, each with a large number of data points, the maximum likelihood estimates (MLEs) would have a multivariate normal distribution, with a mean given by the true values of the parameters and a covariance matrix given by the inverse of the negative of the Hessian of the log-likelihood with respect to the parameters.

It can be shown (see [16]) that the covariance matrix is actually the 'smallest' one possible. This large-sample limiting result is usually a good approximation at finite sample sizes, but it is only valid under some not very restrictive assumptions. The two most important assumptions are: the MLEs must not be at the limit of their possible values; the likelihood must have bounded third derivatives.

3.2 Confidence intervals

Eq (3.3) is easily used to produce confidence intervals (CIs) for parameters, based on the MLEs. For example, suppose that we want an approximate 95% CI for the k^{th} parameter, with MLE $\hat{\theta}_k$. Let $\sigma_{\hat{\theta}_k}$ denote the square root of the k^{th} element on the leading diagonal of $-(\partial^2 l/\partial\boldsymbol{\theta}\partial\boldsymbol{\theta}^T)^{-1}$, then the required 95% CI is $\hat{\theta}_k \pm 1.96\sigma_{\hat{\theta}_k}$. Note that the required Hessian can be obtained analytically or by finite differencing.

A general advantage of the method of maximum likelihood is that the MLEs are invariant under reparameterization of the model. For example, whether we choose to work in terms of Γ_c or a new parameter $\gamma = \Gamma_c^{-1}$, our estimate of Γ_c will be unchanged. This leaves complete freedom to reparameterize for numerical convenience, without modifying statistical conclusions about the most likely parameter values. Unfortunately this invariance need not be shared by the confidence intervals just discussed.

An intuitively unappealing consequence of this lack of invariance is that our confidence intervals can include some parameter values with a lower likelihood than some parameter values outside the confidence intervals. For this reason it could be better to use as confidence intervals those ranges of parameter values that yield highest likelihood.

This can be obtained as follows. Suppose that we wanted to test the hypothesis that $\theta_k=\theta_0$, where θ_0 is a particular value. Now estimate $\boldsymbol{\theta}$ by maximizing the likelihood under the restriction $\theta_k=\theta_0$. Denote the resulting restricted MLE $\hat{\boldsymbol{\theta}}_0$, and let $\hat{\boldsymbol{\theta}}$ denote the MLE obtained without restriction. It turns out that if the hypothesis is true then the probability distribution of the difference in maximized log likelihoods, with and without restriction, is known.

Let λ be defined as twice the difference in the log likelihoods with and without the restriction, such that

$$\lambda=2\{l(\hat{\boldsymbol{\theta}})-l(\hat{\boldsymbol{\theta}}_0)\} \tag{3.4}$$

If the restriction $\theta_k=\theta_0$ is actually the true state of nature then, in the large-sample limit, $\lambda \sim \chi^2_1$. That is, λ has a χ^2 distribution with one degree of freedom (see [15]). In statistical terms we would accept the hypothesis $\theta_k=\theta_0$ at the 5% level if λ was within the smallest 95% of χ^2_1 random variables, i.e. if $\lambda < 3.84$. Otherwise we would reject as the observed λ would appear to be too large to have come from the distribution that should apply if the hypothesis were correct.

Finding a 95% CI is now very simple, conceptually: we simply search for the range of θ_0 values that would be accepted in this hypothesis test. Computationally this search is slightly more complicated than the intervals based on eq (3.3), but the resulting intervals are always invariant.

In the work described below, the log likelihood for each model was coded up in the R statistical language (see [20]). The numerical root-finding required for this was done using the R function *uniroot*. The log likelihoods were maximized using R function *optim* to find the MLEs together with the Hessian of the log likelihood and the log likelihood of the MLE. Both types of confidence interval were also computed in R, with a simple search algorithm used for the invariant intervals. Only the CI calculated by the latter method is shown in the following sections.

4. NUMERICAL VALIDATION OF STATISTICAL APPROACH

In this section, numerical simulation of experimental data is used to examine the characteristics of the statistical estimates. The theoretical curve (referred to below as the 'true curve') for the variation of ε with Φ_o was calculated from eq (2.9) for EI ingress, from which n discrete data points (ϕ_j,e_j) were determined. A normally-distributed error, δ_j, was added to e_j, and the variance of the distribution was σ^2. For the 'tests' reported here, σ = 0.01 and 0.02, and the values of Φ_{min} and Γ_c (referred to as the 'true values') were 0.25 and 0.5 respectively; these are typical values for EI ingress. As for Section 3, the EI subscript has been omitted for simplicity.

An initial set of n = 32 data points was generated and the MLEs (maximum likelihood estimates) of $\hat{\Phi}_{min}$, $\hat{\Gamma}_c$, were calculated together with their upper and lower bounds, which were determined from the confidence intervals. The errors δ_Φ and δ_Γ were defined as the percentage differences between the estimated and true values of Φ_{min} and Γ_c.

Removing alternate data points, the process was repeated for n =16, 8 and 4. For each value of n, the simulated tests were repeated m times and the ensemble averages, $\bar{\Phi}_{min}$, $\bar{\Gamma}_c$, were calculated together with the respective standard deviations, σ_Φ, σ_Γ, between the individual estimates and the ensemble averages.

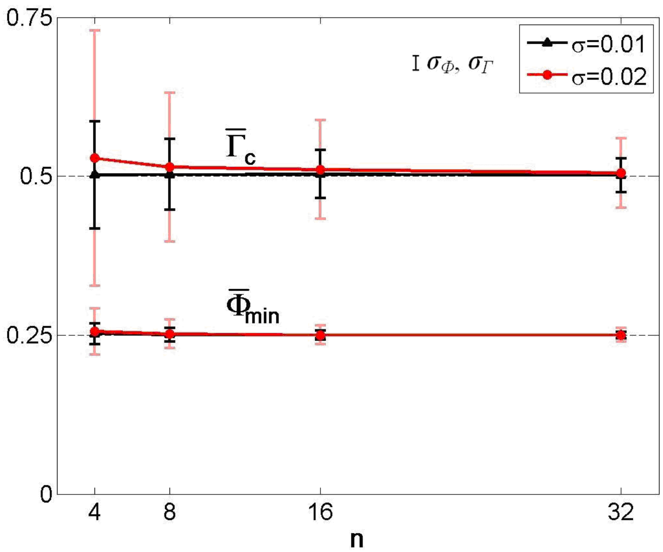

Fig. 5 Variation of $\bar{\Phi}_{min}$, $\bar{\Gamma}_c$ and their standard deviations with n for m = 1000. (Error bars show standard deviations between individual estimates and ensemble averages.)

Fig. 5 shows the variation of $\bar{\Phi}_{min}$, $\bar{\Gamma}_c$ and σ_Φ, σ_Γ with n for m = 1000. It can be seen that $\bar{\Phi}_{min}$, $\bar{\Gamma}_c$ tend to their true values as n increases, but at the smaller values of n there is a bias in the average values. The bias is attributed to the fact that the effectiveness equations are nonlinear: although the errors in ε are normally distributed about the mean, the errors in $\bar{\Phi}_{min}$, $\bar{\Gamma}_c$ are not.

It can also be seen from Fig. 5 that the standard deviations, which are relatively large (particularly for Γ_c) at the smaller values of n, decrease as n increases. A large standard deviation implies high variability between the values obtained from individual tests. It is therefore possible that, for some tests, the estimated value for a single test for n = 4 could, by chance, be more accurate than one for n = 32; but one could never know that this was the case and on average the reverse would be true.

Table 1 shows the results for three particular tests selected from 1000 individual tests with $\sigma=0.01$. Table 1(a) shows typical results where the accuracy of $\hat{\Phi}_{min}$, $\hat{\Gamma}_c$ increase as n increases. Table 1(b) shows atypical results where the accuracy for the n = 4 test is better than that for n = 32. Table 1(c) shows another atypical case where only the confidence intervals for the n = 32 test capture the true values.

For m = 1000 tests, the confidence intervals for n = 4, 8, 16 and 32 did not capture the true value 22.9, 10.8, 8.0 and 6.6% of the tests respectively. If the confidence intervals had been working perfectly then they should have failed to capture the truth on 5% of occasions. The rapidly improving performance as n increases illustrates the rapid improvement with increasing sample size of the large-sample approximations, eqs (3.3) and (3.4), on which the confidence intervals are based. However the results illustrate that insufficient numbers of data points not only produce a significant proportion of inaccurate estimates but also that they could produce confidence intervals that fail to capture the true value. The unwary experimenter would be living in a fool's paradise!

n	$\hat{\Phi}_{min}$	$\hat{\Phi}_{min}^-$	$\hat{\Phi}_{min}^+$	δ_Φ	$\hat{\Gamma}_c$	$\hat{\Gamma}_c^-$	$\hat{\Gamma}_c^+$	δ_Γ
4	0.264	0.245	0.287	5.6%	0.44	0.36	0.53	13%
8	0.254	0.241	0.269	1.8%	0.48	0.41	0.55	4.9%
16	0.252	0.243	0.263	1.0%	0.48	0.44	0.53	3.5%
32	0.249	0.242	0.256	0.5%	0.50	0.46	0.54	0.3%

Test (a)

n	$\hat{\Phi}_{min}$	$\hat{\Phi}_{min}^-$	$\hat{\Phi}_{min}^+$	δ_Φ	$\hat{\Gamma}_c$	$\hat{\Gamma}_c^-$	$\hat{\Gamma}_c^+$	δ_Γ
4	0.254	0.228	0.288	1.5%	0.50	0.36	0.67	1.0%
8	0.253	0.239	0.269	1.3%	0.51	0.44	0.60	2.3%
16	0.247	0.238	0.258	1.0%	0.54	0.48	0.60	7.8%
32	0.244	0.237	0.252	2.3%	0.54	0.50	0.59	8.6%

Test (b)

n	$\hat{\Phi}_{min}$	$\hat{\Phi}_{min}^-$	$\hat{\Phi}_{min}^+$	δ_Φ	$\hat{\Gamma}_c$	$\hat{\Gamma}_c^-$	$\hat{\Gamma}_c^+$	δ_Γ
4	0.222	0.210	0.235	11%	0.73	0.61	0.87	46%
8	0.232	0.220	0.245	7.1%	0.61	0.53	0.72	23%
16	0.237	0.227	0.248	5.3%	0.58	0.52	0.66	16%
32	0.243	0.233	0.255	2.7%	0.55	0.48	0.61	9%

Test (c)

Table 1. Some estimated values for Φ_{min}=0.25, Γ_c=0.5, σ=0.01 (+/- denote upper/lower bounds of 95% confidence intervals.)

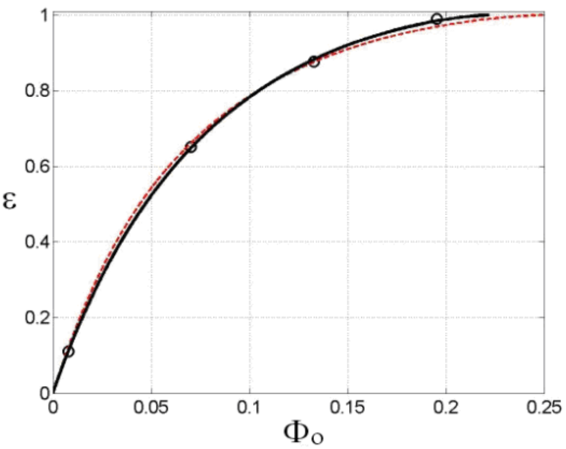

(a) n = 4

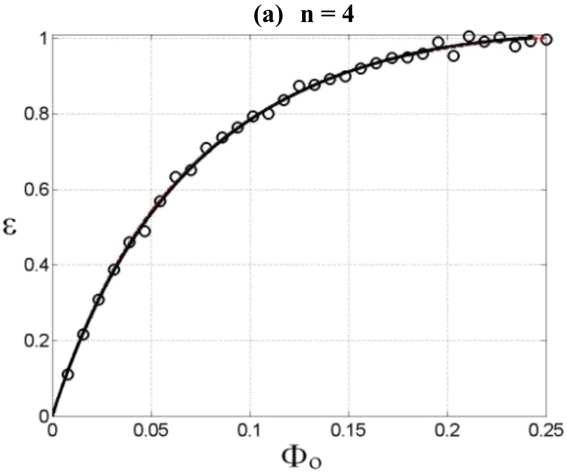

(b) n = 32

Fig. 6 Variation of ε with Φ_o for test (c) in Table 1 Black circles – simulated data; black solid line – fitted curve; red dashed line – true curve.

The danger of drawing conclusions from insufficient data points is illustrated by Fig. 6, which shows the variation of ε with Φ_o for test (c) in Table 1. For n = 4, the fitted curve passes through most of the data points, which could create the belief that the data were good and that the estimated values of $\hat{\Phi}_{min}$, $\hat{\Gamma}_c$ and their confidence intervals were reasonably accurate. However, as revealed by the true curve and by the results in Table 1(c), this conclusion would be wide of the mark! By contrast, the fitted curve for n = 32 in Fig. 6 is much closer to the true curve, and the data in Table 1(c) are much closer to the true values.

In this section, the simulated estimates were compared with theoretical curves, and the theoretical model was implicitly assumed to provide the true answers. In practice, the true answers are unknown and the theoretical model is just that: a model. In the next section, the theoretical and statistical models are applied to real experimental data, and the interpretation of the results will be tempered by the caveats revealed by the above simulations.

5. FITTING THEORETICAL CURVES TO EXPERIMENTAL DATA

In Section 4, the statistical model was tested using noisy data generated from the EI effectiveness curve. The experimental data used in this section provides tests for both the statistical and the theoretical model.

.

5.1 Rotationally-induced (RI) ingress

In [1], Owen validated the orifice model for RI ingress using the experimental data of Graber *et al.* [6]. Graber *et al.* used concentration measurements to determine the sealing effectiveness ε for several rim-seal geometries in a rig in which the axial velocity in the annulus was very small (< 33 cm/s) and the swirl ratio in the mainstream flow in the external annulus ($V_{\phi,2}/\Omega b$) could be varied. Graber *et al.* plotted their measured values of ε versus η_t, a sealing flow parameter where

$$\eta_t = 0.5\, G_c\, Re_\phi^{\;0.2}\, \Phi_o \qquad (5.1)$$

For ease of correlation with the theoretical curves, the experimental data shown in Figs 7-9 were obtained by replotting the data shown in [6] versus Φ_o; the data for $\Phi_{i,RI}$ - which were not included in [6] - were obtained using eq (2.6). It should be pointed out that the data for Fig. 8 were obtained from two separate figures in [6], corresponding to the two different values of G_c, and the data for Fig. 9 were obtained from separate figures in [6] for the two values of Re_ϕ. (Instead of having to use separate correlations for the effects of G_c and Re_ϕ on ε, Φ_o combines $C_{w,o}$, G_c and Re_ϕ into a single flow parameter.)

For the cases discussed here, the statistical model described above was used to determine the optimum values of $\Phi_{min,RI}$ and Γ_c. By contrast, Owen *assumed* values for these two parameters: for $\Phi_{min,RI}$, he used the Bayley-Owen correlation given in eq (2.1), which is equivalent to $\Phi_{min,RI} = 0.097$, and for simplicity he assumed that $\Gamma_c = 1$. The theoretical curves for ε, based on these two assumed values, are also shown in Fig. 7 - Fig. 9; no theoretical curves for $\Phi_{i,RI}$ were shown by Owen.

Table 2 includes the values of Γ_c, $\Phi_{min,RI}$ (together with their upper and lower bounds) and $\Phi_{i,RI}$* obtained from the correlations. Owing to the relatively large uncertainty in the experimental data, the confidence intervals are also relatively large. $\Phi_{i,RI}$* was calculated from eq (2.7); it is the maximum value of $\Phi_{i,RI}$, which occurs when Φ_o = 0; this theoretical value cannot be readily determined from concentration measurements.

Fig. 7 shows a comparison between the theoretical curves and the experimental data for the case of an axial-clearance seal with a clearance ratio of G_c=0.00476 and a rotational Reynolds number of Re_ϕ=5.1×10^6. A thumb-nail sketch of the seal configuration is shown on this and the following two figures, and it should be noted that the external flow is from right to left (*i.e.* from the rotor towards the stator). Two levels of external swirl were used in the experiment: $V_{\phi,2}/\Omega b$=1 and 2.

It can be seen from Fig. 7 that there is no systematic effect of external swirl on the effectiveness and that the theoretical correlation for ε is only marginally better than Owen's curve. Table 2 shows that $\Phi_{min,RI} = 0.105$, which is reasonably close to the Bayley-Owen value of 0.097. Table 2 also shows that, owing to the relatively large values of σ, the confidence intervals in $\Phi_{min,RI}$ are relatively large. (The reasonable agreement between the Graber *et al.* and the Bayley and Owen values of $\Phi_{min,RI}$ may be fortuitous as the Bayley-Owen correlation was based on pressure measurements!)

Fig. 8 shows the correlations for a radial-clearance seal for two clearance ratios. For this case, the fitted curve for ε is significantly better than Owen's curve; Table 2 shows that the optimum value of $\Phi_{min,RI} = 0.122$, which is higher than the Bayley-Owen value of 0.097. (As pointed out in [1], it is surprising that – unlike the RI data of Phadke and Owen [7] - $\Phi_{min,RI}$ for the radial-clearance seals is larger than that for the axial-clearance seal. However, it should be noted that the radial-clearance seals of Graber *et al.* corresponded to those in the aft wheel-space, downstream of the turbine blades.)

Fig. 9 shows the correlations for a radial-clearance seal for two rotational Reynolds numbers. Once again, the fitted curve for ε is significantly better than Owen's curve. Table 2 shows that $\Phi_{min,RI}$ =0.157, but again the confidence interval for $\Phi_{min,RI}$ is relatively large.

	$\hat{\Phi}_{min}$	$\hat{\Phi}_{min}^{-}$	$\hat{\Phi}_{min}^{+}$	$\Phi_{i,RI}^{*}$	$\hat{\Gamma}_c$	$\hat{\Gamma}_c^{-}$	$\hat{\Gamma}_c^{+}$	σ
Fig.7	0.105	0.085	0.142	0.0283	0.64	0.37	1.28	0.049
Fig.8	0.122	0.094	0.183	0.0227	0.4	0.22	0.70	0.032
Fig.9	0.157	0.13	0.206	0.0272	0.37	0.25	0.5	0.036

Table 2: Values of estimated parameters corresponding to Fig. 7 to 9 for RI ingress. (+/- denote upper/lower bounds of 95% confidence intervals.)

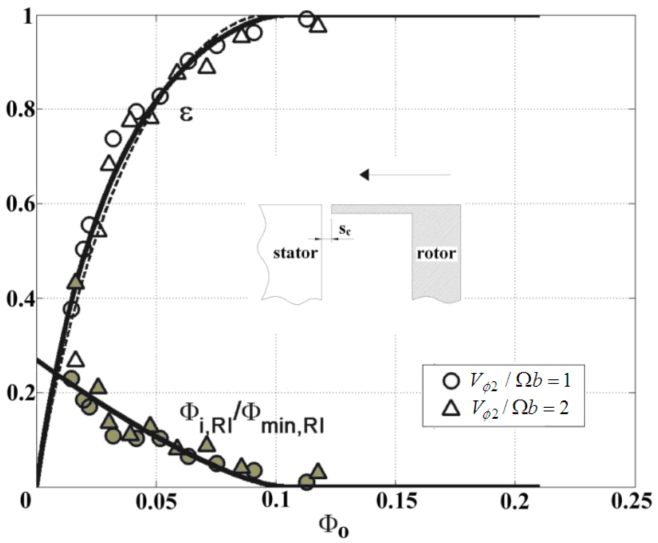

Fig. 7 Comparison between theoretical curves and experimental data of Graber *et al.* [6] for axial-clearance seal: $G_c = 0.00476$, $Re_\phi = 5.1 \times 10^6$. (Open symbols are ε data; closed symbols are $\Phi_{i,RI}/\Phi_{min,RI}$ data; solid lines are theoretical curves; broken line is theoretical curve of Owen [1].)

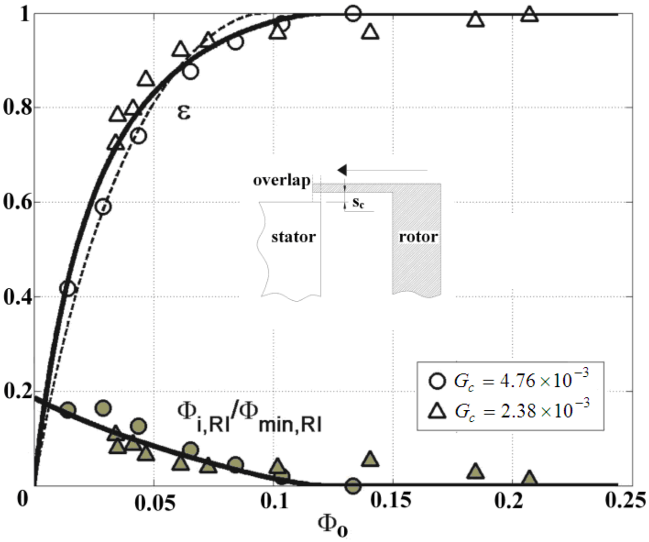

Fig. 8 Comparison between theoretical curves and experimental data of Graber *et al.* [6] for radial-clearance seals: G_c = 0.00238 and 0.00476, Re_ϕ = 2.6 × 10^6. (Open symbols are ε data; closed symbols are $\Phi_{i,RI}/\Phi_{min,RI}$ data; solid lines are theoretical curves; broken line is theoretical curve of Owen [1].)

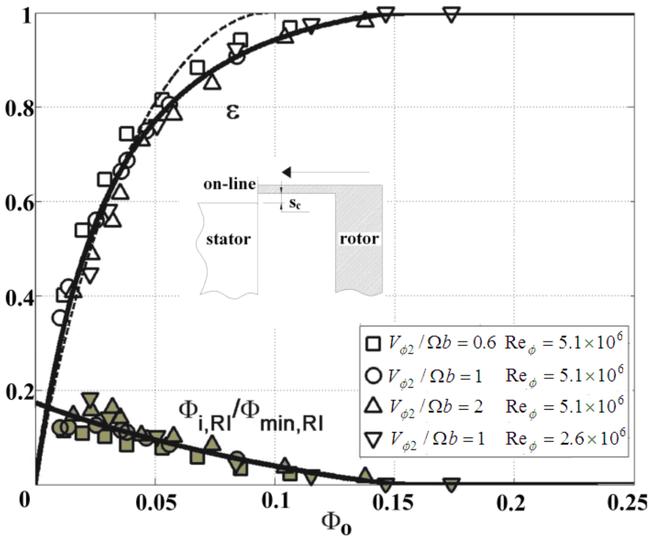

Fig. 9 Comparison between theoretical curves and experimental data of Graber *et al.* [6] for radial-clearance seal: G_c = 0.00476, Re_ϕ = 2.6 × 10^6 and 5.2 × 10^6 (Open symbols are ε data; closed symbols are $\Phi_{i,RI}/\Phi_{min,RI}$ data; solid lines are theoretical curves; broken line is theoretical curve of Owen [1].)

5.2 Externally-induced (EI) ingress

The effectiveness data used for the correlations in Fig. 10 and 11 were respectively based on the CFD (computational fluid dynamics) data given by Owen *et al.*[3] and on the concentration measurements presented by Johnson *et al.* [12]. The $\Phi_{i,EI}$ data - which were not determined in either of these papers - were calculated here using eq (2.10). Table 3 includes the values of Γ_c, $\Phi_{min,EI}$ (together with their upper and lower bounds); $\Phi_{i,EI}*$ was calculated from eq (2.12). ($\Phi_{i,EI}*$is the maximum value of $\Phi_{i,EI}$, which occurs when $\Phi_o=0$; this theoretical value cannot be readily determined from concentration measurements.) Owing to the sparseness of the data, the confidence intervals are relatively large.

The CFD effectiveness data in [3] were obtained using a steady 3D code for an axial-clearance seal in which there were stationary vanes in the annulus upstream of the seal but no rotating blades downstream. In [3], the ε-data were fitted using a least-squares method, from which Γ_c and $\Phi_{min,EI}$ were determined.

In Fig. 10, the method described in Section 3 is used to fit the effectiveness equation. Although eqs (2.9) and (2.11) provide a very good fit to the CFD data, Table 3 shows that, owing to the limited number of data points, the confidence interval for $\Phi_{min,EI}$ is relatively large. Despite this, the values of Γ_c and $\Phi_{min,EI}$ in Table 3 agree with those found in [3].

Fig. 11 shows very good agreement between the theoretical curves, eqs (2.9) and (2.11), and the experimental data of Johnson *et al.* The latter authors used an orifice model, which they solved numerically for different values of $C_{d,e}$ and $C_{d,i}$. They achieved the best fit to their effectiveness data with $C_{d,e}$ = 0.27 and $C_{d,i}$ = 0.20, corresponding to Γ_c = 0.74; this value is well within the confidence interval of the estimated value of Γ_c = 0.69 in Table 3. It should be noted however that, as $n = 7$, there is a question about the accuracy of these values and of the estimated value of $\Phi_{i,EI}$.

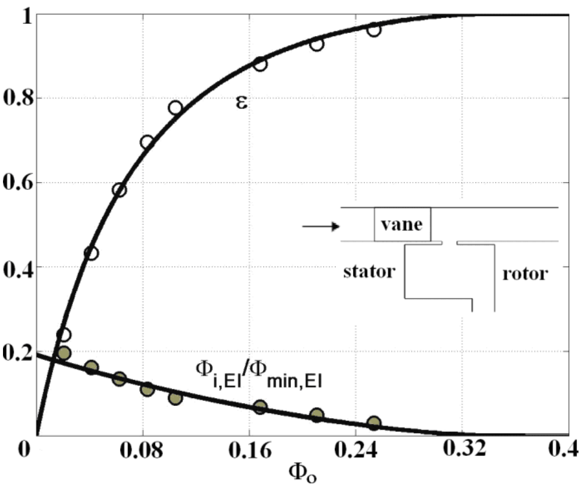

Fig. 10 Comparison between theoretical curves and CFD data of Owen *et al.* [3] for axial-clearance seal: G_c = 0.01, Re_ϕ= 1.03 × 10^6. (Open symbols are ε data; closed symbols are $\Phi_{i,EI}/\Phi_{min,EI}$ data; solid lines are theoretical curves.)

	$\hat{\Phi}_{min}$	$\hat{\Phi}_{min}^{-}$	$\hat{\Phi}_{min}^{+}$	$\Phi_{i,RI}*$	$\hat{\Gamma}_c$	$\hat{\Gamma}_c^{-}$	$\hat{\Gamma}_c^{+}$	σ
Fig.10	**0.335**	**0.282**	**0.415**	**0.064**	**0.35**	**0.23**	**0.51**	**0.016**
Fig.11	**0.170**	**0.152**	**0.195**	**0.049**	**0.69**	**0.48**	**0.96**	**0.012**

Table 3: Values of estimated parameters corresponding to Fig. 10 and 11 for EI ingress. (+/- denote upper/lower bounds of 95% confidence intervals.)

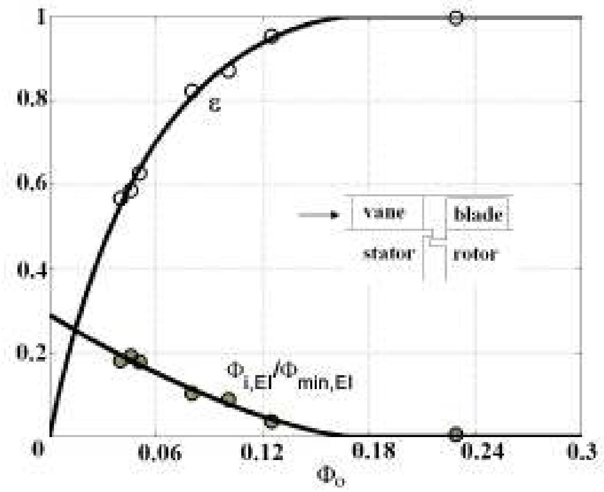

Fig. 11 Comparison between theoretical curves and experimental data of Johnson *et al.* [9] for single-overlap seal: G_c=0.01, Re_ϕ= 0.59 × 10^6. (Open symbols are ε data; closed symbols are $\Phi_{i,EI}/\Phi_{min,EI}$ data; solid lines are theoretical curves.)

6.CONCLUSIONS

The statistical method of maximum likelihood estimation was used to fit the effectiveness equations for EI and RI ingress to previously-published experimental data and to determine the optimum values of the two empirical constants, Φ_{min} and Γ_c.

The statistical method was validated using simulated noisy data generated from the EI effectiveness equation. Using repeated tests, it was shown that the accuracy of individual estimates of Φ_{min} and Γ_c increased and the variability decreased as n (the number of data points in each test) increased. For $n \geq 16$ the simulations showed that the estimated values of Φ_{min} and Γ_c were in acceptably close agreement with the 'true values', and the confidence intervals captured the true values in over 90% of the test cases. For $n \leq 8$, there was increased variability, reduced accuracy and the estimated confidence intervals were less reliable.

For RI ingress, maximum likelihood estimation was used in conjunction with the effectiveness equations to fit the experimental data of Graber et al [6]. The agreement between the effectiveness equation and the data was significantly better than that obtained by Owen [1], who *assumed* values for Γ_c and Φ_{min}. However, owing to the relatively large experimental uncertainties, the confidence intervals for the estimated values of Γ_c and Φ_{min} were relatively large. The theoretical distribution of Φ_i, the nondimensional ingested flow rate, agreed closely with the values derived from the experimental data.

For EI ingress, the methods were used to fit the effectiveness curve to the computational data of Owen et al [3] and the experimental data of Johnson et al [12]. In both cases, the agreement between the fitted curves and the data was very good. However, owing to the limited number of data points, there is no guaranty that the confidence intervals captured the true values.

Sangan et al [13, 14] have recently obtained very good agreement between the statistical and theoretical models described here and data obtained from a new experimental rig at the University of Bath. It is the ultimate aim of this research to determine the relative performance of different seal geometries and to apply the effectiveness data obtained at rig conditions to engine-operating conditions.

ACKNOWLEDGEMENTS

We wish to thank the China Scholarship Council and Beihang University, Beijing, China, for supporting Kunyuan Zhou during his stay at the University of Bath. The research described here is part of a programme jointly funded by the UK Engineering and Physical Sciences Research Council, Siemens Fossil Power Generation and Siemens Oil & Gas.

REFERENCES

1. Owen, J.M., 2011, “Prediction of Ingestion Through Turbine Rim Seals---Part I: Rotationally Induced Ingress”; ASME J. Turbomach., Vol. 133, Issue 3, 031005-1 to 9.
2. Owen, J.M., 2011, “Prediction of Ingestion Through Turbine Rim Seals---Part II: Externally Induced and Combined Ingress”; ASME J. Turbomach., Vol. 133, Issue 3, 031006-1 to 9.
3. Owen, J.M., Zhou, K., Pountney, O., Wilson, M. and Lock, G.D., 2010, “Prediction of Ingress through Turbine Rim Seals. Part 1: Externally-Induced Ingress”; ASME Paper GT2010-23346. To appear in ASME J Turbomach.
4. Owen, J.M., Pountney, O., and Lock, G.D., 2010, “Prediction of Ingress through Turbine Rim Seals. Part 2: Combined Ingress”; ASME Paper GT2010-23349. To appear in ASME J Turbomach.
5. Bayley, F.J. and Owen, J.M., 1970, “The Fluid Dynamics of a Shrouded Disk System with a Radial Outflow of Coolant”; ASME J Eng Power, 92, pp. 335-341.
6. Graber, D.J., Daniels, W. A and Johnson, B V., 1987, “Disk Pumping Test, Final Report”; Air Force Wright Aeronautical Laboratories, Report No. AFWAL-TR-87-2050.
7. Phadke, U.P. and Owen, J.M., 1988, “Aerodynamic Aspects of the Sealing of Gas-Turbine Rotor-Stator Systems, Part 1: The Behaviour of Simple Shrouded Rotating-Disk Systems in a Quiescent Environment”; Int J Heat Fluid Flow, 9, pp 98-105.
8. Phadke, U.P. and Owen, J.M., 1988, “Aerodynamic Aspects of the Sealing of Gas-Turbine Rotor-Stator Systems, Part 2: The Performance of Simple Seals in a Quasi-Axisymmetric External Flow”; Int J Heat Fluid Flow, 9, pp 106-112.
9. Phadke, U.P. and Owen, J.M., 1988, “Aerodynamic Aspects of the Sealing of Gas-Turbine Rotor-Stator Systems, Part 3: The Effect of Non-Axisymmetric External Flow on Seal Performance”; Int J Heat Fluid Flow, 9, pp 113-117.
10. Johnson, B.V., Jakoby, R., Bohn, D.E. and Cunat, D., 2009, “A Method for Estimating the Influence of Time-Dependent Vane and Blade Pressure Fields on Turbine Rim Seal Ingestion”; ASME J.Turbomach., Vol. 131, Issue 2, 021005-1 to 10.
11. Bohn, D. and Wolff, M., 2003, “Improved Formulation to Determine Minimum Sealing Flow -Cw,min for Different Sealing Configurations”; ASME-Paper GT2003-38465.
12. Johnson, B.V., Cheng-Zhang Wang and Roy, P.R., 2008, “A Rim Seal Orifice Model with Two Cds and Effect of Swirl in Seals”; ASME Paper GT2008-50650.
13. Sangan, C.M., Pountney, O.J., Zhou, K., Wilson, M., Owen, J.M. and Lock, G.D., 2011, “Experimental Measurements of Ingress through Turbine Rim Seals. Part 1: Externally-Induced Ingress”; ASME Paper GT2011-45310.
14. Sangan, C.M., Pountney, O.J., Zhou, K., Wilson, M., Owen, J.M. and Lock, G.D., 2011, “Experimental Measurements of Ingress through Turbine Rim Seals. Part 2: Rotationally-Induced Ingress”; ASME Paper GT2011-45313.
15. Wood, S.N., 2006, “Generalized Additive Models: An Introduction with R”; Chapman and Hall/CRC, Boca Raton, Florida.
16. Silvey, S.D., 1975, “Statistical Inference”; Chapman & Hall, London.
17. Davison, A.C., 2003, “Statistical Models”; Cambridge University Press, Cambridge.
18. Press, W.H., Teukolsky, S.A., Vetterling, W.T. and Flannery, B.P. , 2007, “Numerical Recipes”; Cambridge University Press, Cambridge.
19. Nocedal, J. and Wright, S.J., 2006, “Numerical optimization”; Springer, New York.
20. R.Development.Core.Team, 2010, “A Language and Environment for Statistical Computing”; R Foundation for Statistical Computing, Vienna, Austria. ISBN 3-900051-07-0, URL http://www.R-project.org.

